X. Chen

Department of Civil Engineering and Engineering
Mechanics,
Columbia University,
New York, NY 10027
Mem. ASME

John W. Hutchinson

Division of Engineering and Applied Sciences,
Harvard University,
Cambridge, MA 02138
Fellow ASME

Herringbone Buckling Patterns of Compressed Thin Films on Compliant Substrates

A thin metal film vapor deposited on thick elastomer substrate develops an equi-biaxial compressive stress state when the system is cooled due to the large thermal expansion mismatch between the elastomer and the metal. At a critical stress, the film undergoes buckling into a family of modes with short wavelengths characteristic of a thin plate on a compliant elastic foundation. As the system is further cooled, a highly ordered herringbone pattern has been observed to develop. Here it is shown that the herringbone mode constitutes a minimum energy configuration among a limited set of competing modes. [DOI: 10.1115/1.1756141]
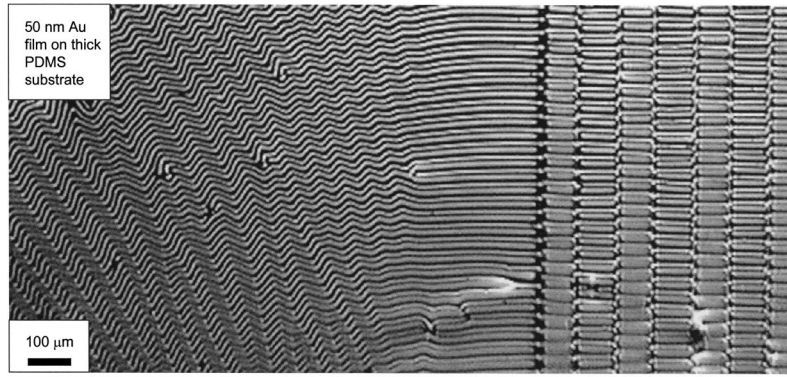
1 Introduction

Recent studies (Bowden et al. [1], Huck et al. [2], and Yoo et al. [3]) have explored the feasibility of manipulating buckled films on compliant substrates to achieve highly ordered patterns with distinctive features. A metal film with a thickness measured in tens of nanometers can be vapor deposited at an elevated temperature on a thick elastomer substrate. When the film/substrate system is cooled, the large mismatch between the thermal expansion of the metal and elastomer produces a state of equi-biaxial compression in the film. At a critical temperature the film begins to buckle into modes with wavelengths typically measured in microns. As the temperature is further lowered the amplitude of the buckles grow and distinctive patterns emerge. Buckle patterns can be manipulated either by creating nonplanar substrate topography prior to deposition, [1,2], or by forcing a film on a smooth planar substrate to buckle into a nonplanar mold that is subsequently removed, [3]. If the surface of the substrate is nonplanar at the start of deposition, the buckle pattern is influenced by the underlying topography. On the right-hand side of Fig. 1, one sees the buckle pattern that arises when the substrate surface has a series of flat depressions running linearly in the vertical direction. Due to local deformation of the substrate, the in-plane film stress is relaxed in the direction perpendicular to the edges of the depressions resulting in the buckle alignment shown, [1,2]. This alignment persists well beyond the left-most depression edge in Fig. 1 where the substrate is perfectly smooth and flat prior to buckling. The parallel undulations in the left-center of Fig. 1 transition to the herringbone pattern. The herringbone buckle pattern appears to be the preferred mode whenever there exists a sufficiently large patch of smooth substrate and when the system has been cooled well below the onset of buckling. There are irregularities to the herringbone pattern, including local distortion most likely due to imperfections in either the film or substrate. Another example is shown in Fig. 2 where the substrate is pre-patterned with a single circular depression of several millimeters diameter at its center. The depression edge determines the orientation of the buckles in its vicinity, but away from the edge the herringbone pattern emerges. The example in Fig. 3, which is taken from [3], shows the highly ordered mode that forms when a mold with a square

pattern is held against the film as the buckles form and is then removed when the buckles are fully developed. In this case the film is aluminum and the substrate has two layers, a relatively thin compliant polymer layer (polystyrene) bonded to a thick silicon layer.

All the films considered in this paper remain bonded to the substrate in the buckled state. They undergo little, or no, plastic deformation. Selected tests revealed that the buckles almost entirely disappeared when the temperature was reversed, [1,2]. The fact that the film locks into modes that are very different from what would be expected from a linear buckling analysis is due to the highly nonlinear character of buckling of an elastic film on a compliant substrate as the temperature drops well below critical. Nonlinearity also accounts for the unusual, highly ordered herringbone mode of buckling in Figs. 1 and 2 that is observed when the system is not manipulated in any way. In Figs. 1 and 2, the substrate is the elastomer, polydimethylsiloxane, (or PDMS, for short) and the film is 50 nm of gold. The crest-to-crest separation of the buckle undulations or ''waves'' is about 30 μm and the distance between jogs in the herringbone mode is about 100 μm. The change in direction of the waves at each jog is approximately 90 deg. The amplitude of the waves is on the order of a micron or smaller. Thus, although the amplitude is large compared to the film thickness, the mode is shallow in the sense that the slopes of the pattern are small. The strains associated with the buckling mode are also small, and both the film and the substrate materials are within their respective linear elastic ranges.

The herringbone pattern is very different from any mode one might suspect based on a linear stability analysis, as will be seen later. A clue to its existence is its ability to alleviate equally in all directions the biaxial in-plane stress driving buckling. A mode with undulations extending in only one direction such as that seen on the right in Fig. 1, which will be referred to as a *one-dimensional mode*, relieves in-plane stress only in the direction perpendicular to the undulations. The in-plane stress component parallel to the undulations is only slightly altered by buckling. On the other hand, the alternating directions of the local one-dimensional undulations in the herringbone mode reduce the overall in-plane stress in the film in all directions. The herringbone mode allows for an isotropic average in-plane expansion of the film, but otherwise has zero Gaussian curvature apart from the vicinity of the jogs. In addition to bending, some nonuniform stretching of the film necessarily occurs locally at the jogs. Nevertheless, the near-inextensionality (apart from the average uniform expansion) of the herringbone mode and its ability to alleviate the in-plane stress equally in all directions are the two features underlying its preferred existence. An origami pattern similar to it can be created from a series of folds of a piece of paper.

Fig. 1 Buckling of a 50 nm gold film on a thick elastomer (PDMS) substrate. On the right, the substrate has been patterned with alternating flat depressions, [2]. The substrate on the left two-thirds of the figure is flat and not patterned. The herringbone pattern is on the left. The wavelength of the pattern across the crests is approximately 30 μm while the distance between jogs of the herringbone mode is approximately 100 μm.

It will be shown that the herringbone mode of buckling is the minimum energy configuration among several competing modes. We confine attention to modes that are periodic, and we begin by presenting the result of the classical buckling analysis for the family of modes associated with the critical stress. Then, a closed-form analysis is presented of one-dimension undulations of finite amplitude at temperatures arbitrarily below the critical stress. Numerical analyses of the herringbone mode and a square checkerboard mode follow. The film is represented as an elastic thin plate satisfying the nonlinear von Karman plate equations. These equations are accurate for the shallow modes observed. In the analytical work, the elastomer substrate is represented by linear, small strain elasticity theory. This is an accurate representation because the strains in the substrate remain small. Moreover, a linear strain-displacement characterization of the substrate is justified because

the substrate experiences no pre-stress—buckling is driven by the pre-stress in the film not the substrate. In the numerical analysis of the two other modes, nonlinear kinematics holds throughout the system (with linear stress-strain behavior), but nonlinearity in the substrate is negligible. It will be seen that the energy associated with the herringbone mode is distinctly below that of the other two modes. The energy minimum of the herringbone pattern is relatively flat in the sense that there is little change in the energy for a fairly wide range of the parameters characterizing the geometry of the pattern, especially the spacing between jogs. The paper ends with speculation on how the mode forms and a discussion on the limitations of approaches based on energy minimization.

The Young's modulus, Poisson's ratio and coefficient of thermal expansion of the film are denoted by E, ν, and α. The corresponding quantities for the substrate are denoted by E_s, ν_s, and α_s. The film thickness is t. The substrate is assumed to be infinitely thick and, thus, it imposes its in-plane strains on the film. Assuming the film is deposited on the substrate when both are at temperature T_D and the temperature of the system is then reduced by ΔT, and assuming the film is elastic and unbuckled, the compressive equi-biaxial pre-stress stress, σ_0, in the film is

$$\sigma_{11} = \sigma_{22} = -\sigma_0 = -[E/(1-\nu)] \int_{T_D - \Delta T}^{T_D} \Delta \alpha \, dT \qquad (1)$$

where $\Delta \alpha = \alpha_s - \alpha$. For the systems under consideration, $\Delta \alpha > 0$ and $\sigma_0 > 0$.

The von Karman plate equations, [4], governing the deflection of the film are

$$D \nabla^4 w - (N_{11} w_{,11} + N_{22} w_{,22} + 2 N_{12} w_{,12}) = -p \qquad (2)$$

$$\frac{1}{Et} \nabla^4 F = w_{,12}^2 - w_{,11} w_{,22}. \qquad (3)$$

Here, ∇^4 is the bi-harmonic operator, $D = Et^3/[12(1-\nu^2)]$ is the bending stiffness of the plate, w is its displacement perpendicular to the plane, (x_1, x_2), p is the stress component acting perpendicular to the plate that is exerted by the substrate, $(\ )_{,\alpha} \equiv \partial(\ )/\partial x_\alpha$, $N_{\alpha\beta} = \int \sigma_{\alpha\beta} dx_3$ is the stress resultant in the plane of the plate and F is the Airy stress function with $(N_{11} = F_{,22}, \ N_{22} = F_{,11}, \ N_{12} = -F_{,12})$. Equation (2) is the moment equilibrium equation, and (3) is the compatibility equation ensuring the existence of in-plane displacement gradients, $u_{\alpha,\beta}$. Tangential components of the traction exerted by the substrate on the plate are ignored. This is a standard approximation in the analysis of wrinkling of a thin film on compliant substrate, [5], whose accuracy can be validated by a
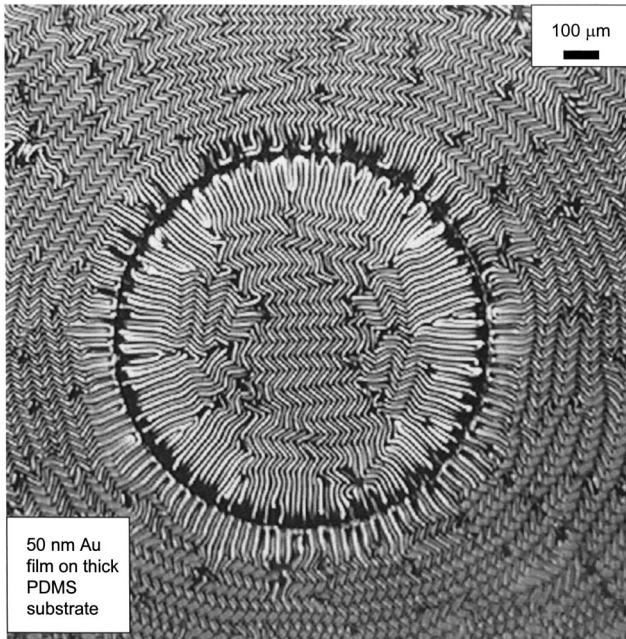
Fig. 2 Gold film on a substrate which has been patterned with a circular flat depression of several millimeters in diameter, [1]. The herringbone pattern emerges in the center of the spot and outside the edges of the spot.
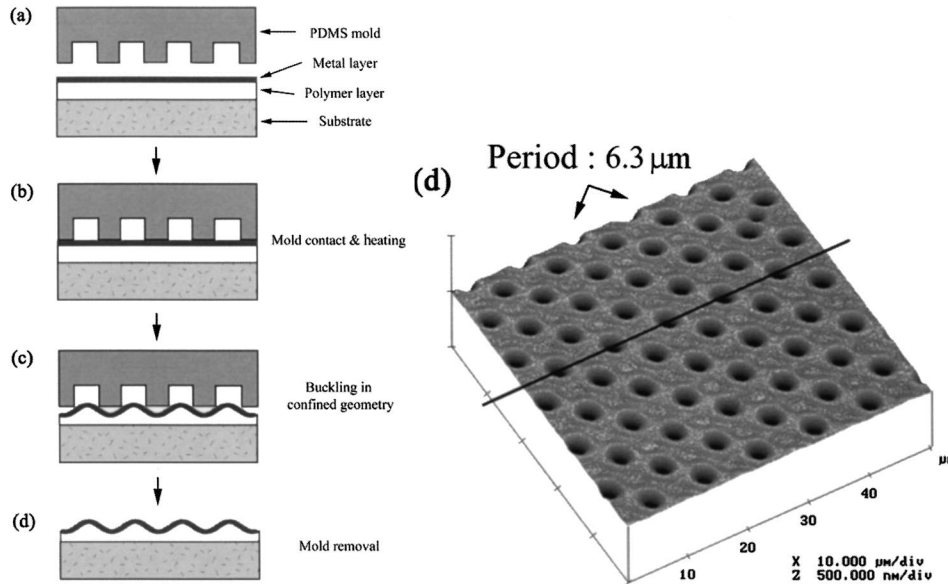
Fig. 3 An example from [3] of a highly organized buckling pattern for a film/substrate system. As depicted, the film is forced to buckle into a mold with a square pattern, after which the mold is removed.

more detailed analysis for one-dimensional modes (see below). Middle surface strains are related to displacements by $E_{\alpha\beta} = 1/2(u_{\alpha,\beta}+u_{\beta,\alpha})+1/2w_{,\alpha}w_{,\beta}$; $N_{\alpha\beta}=[E/(1-\nu^2)]((1-\nu)E_{\alpha\beta}+\nu E_{\gamma\gamma}\delta_{\alpha\beta})$; and $M_{\alpha\beta}=D((1-\nu)w_{,\alpha\beta}+\nu w_{,\gamma\gamma}\delta_{\alpha\beta})$ are the constitutive relations with $M_{\alpha\beta}$ as the bending moment tensor.

2 Classical Buckling Based on Linearized Stability Analysis

The film is imagined to be infinite in extent. The unbuckled film has a uniform stress state given by $N_{11}=N_{22}=-\sigma_0 t$, $N_{12}=0$. The classical buckling analysis, based on linearization of (2) and (3) about the pre-buckling state, leads to

$$D\nabla^4 w + \sigma_0 t \nabla^2 w = -p \qquad (4)$$

along with $\nabla^4 \Delta F = 0$ where $F = -1/2(x_1^2+x_2^2)\sigma_0 t + \Delta F$. The system of equations admits periodic solutions of the form

$$w = \hat{w}\cos(k_1 x_1)\cos(k_2 x_2), \quad p = \hat{p}\cos(k_1 x_1)\cos(k_2 x_2),$$
$$\Delta F = 0 \qquad (5)$$

with (4) giving $(Dk^4 - \sigma_0 t k^2)\hat{w} = -\hat{p}$ where $k = \sqrt{k_1^2+k_2^2}$.

The exact solution for the normal deflection of the surface, δ, of the infinitely deep substrate under the normal loading p in (5) with zero tangential tractions at the surface is $\delta = \hat{\delta}\cos(k_1 x_1)\cos(k_2 x_2)$ where $\hat{\delta}=2\hat{p}/(\bar{E}_s k)$ with $\bar{E}_s = E_s/(1-\nu_s^2)$.[1] Combining $(Dk^4 - \sigma_0 t k^2)\hat{w}=-\hat{p}$ and $\hat{\delta}=2\hat{p}/(\bar{E}_s k)$ subject to $\hat{w}=\hat{\delta}$ gives the eigenvalue equation $\sigma_0 t = Dk^2 + \bar{E}_s/2k$. The critical buckling stress, σ_0^C, is the minimum eigenvalue with respect to k, which is attained for $k^C t = (3\bar{E}_s/\bar{E})^{1/3}$ giving

$$\frac{\sigma_0^C}{\bar{E}} = \frac{1}{4}\left(3\frac{\bar{E}_s}{\bar{E}}\right)^{2/3} \qquad (6)$$

with $\bar{E}=E/(1-\nu^2)$. This is the result for the one-dimensional, plane-strain wrinkling stress, which is widely known, [5]. Note,

---

[1]The effect of the boundary conditions tangential to the surface of the substrate is minor. For example, if the tangential displacements are constrained to be zero, one finds $\hat{\delta}=2\hat{p}\lambda/\bar{E}_s k$ where $\lambda=(3-4\nu_s)/[4(1-\nu_s)^2]$. For $\nu_s=1/3$, $\lambda=15/16$; for $\nu_s=1/2$, $\lambda=1$.

however, for an equi-biaxial pre-stress, the critical stress applies not only to the one-dimensional mode with $k_1=k^C$ and $k_2=0$ but to *any* mode whose wave numbers satisfy

$$\sqrt{k_1^2+k_2^2}\,t = k^C t = (3\bar{E}_s/\bar{E})^{1/3}. \qquad (7)$$

The compressed film in the equi-biaxial state has multiple modes associated the critical buckling stress. In what follows, both the one-dimensional mode and the square checkerboard mode with $k_1=k_2=k^C/\sqrt{2}$ will be investigated.

3 Nonlinear Analysis of the One-Dimensional Mode

An exact closed-form solution for the nonlinear von Karman plate coupled to the linearly elastic foundation is possible for the one-dimensional mode with nonzero k_1 and $k_2=0$. The eigenvalue (i.e., the stress at the onset of buckling) associated with arbitrary k_1 is now denoted by $\sigma_0^E t = Dk_1^2+\bar{E}_s/2k_1$ to distinguish it from the stress in the unbuckled state, σ_0. Results will be presented for various k_1 including the critical case with $k_1=k^C$ and $\sigma_0^E=\sigma_0^C$. The solution is produced for temperatures such that $\sigma_0 > \sigma_0^E$.

The normal displacement in the finite amplitude state continues to be $w=\hat{w}\cos(k_1 x_1)$, and (3) implies that the resultant stress in the buckled film, N_{11}, is independent of x_1. It follows, then, from (2) that the relation $N_{11}=-\sigma_0^E t$ remains in effect in the nonlinear regime. An additional constraint must be imposed to ensure that u_1 is consistent with the overall substrate deformation, i.e., $\int_0^{2\pi/k_1}\Delta u_1 dx_1=0$ where $\Delta u_1 = u_1-u_1^0$ with u_1^0 as the displacement in the unbuckled film at σ_0. (Equation (3) ensures the existence of du_1/dx_1; this condition provides the underdetermined constant, ensuring the overall film displacement matches that of the substrate.) This constraint condition can be expressed using the strain-displacement relation and the stress-strain relation as

$$\frac{1}{\bar{E}t}(\sigma_0 t + N_{11}) = \frac{k_1}{4\pi}\int_0^{2\pi/k_1}\left(\frac{dw}{dx_1}\right)^2 dx_1 = \frac{k_1^2}{4}\hat{w}^2. \qquad (8)$$

Thus, the amplitude of the buckling mode is obtained by combining (8) with $N_{11}=-\sigma_0^E t$:

$$\frac{\hat{w}}{t} = \frac{2}{k_1 t} \sqrt{\frac{(\sigma_0 - \sigma_0^E)}{\bar{E}}}. \tag{9}$$

In the unbuckled state when the film stress is σ_0, the substrate is unstressed and the energy per unit area in the film/substrate system is

$$U_0 = \frac{1-\nu}{E} \sigma_0^2 t. \tag{10}$$

The average energy per unit area in the buckled state can be expressed as

$$U = \frac{1}{2E}(N_{11}(N_{11} - \nu N_{22}) + N_{22}(N_{22} - \nu N_{11}))$$

$$+ \frac{k_1}{4\pi} \int_0^{2\pi/k_1} D\left(\frac{d^2 w}{d^2 x_1}\right)^2 dx_1 + \frac{k_1}{4\pi} \int_0^{2\pi/k_1} pw dx_1. \tag{11}$$

In (11), the first contribution is from the uniform resultant in-plane stresses in the film, the second is the bending contribution from the film, and the third is the elastic energy in the substrate. Enforcing $\Delta E_{22} = 0$, as measured from the unbuckled state at σ_0, one readily finds that $N_{22} = -(1-\nu)\sigma_0 t - \nu\sigma_0^E t$. Each of the contributions in (11) can be evaluated explicitly. In the same order as in (11), the ratios of the energy contributions in the buckled state to the energy in the unbuckled state are

$$\frac{U}{U_0} = \frac{1+\nu}{2}\left[\left(\frac{\sigma_0^E}{\sigma_0}\right)^2 + \frac{(1-\nu)^2}{(1-\nu^2)}\right] + \frac{(1+\nu)(k_1 t)^4}{48}\left(\frac{\bar{E}}{\sigma_0}\right)^2\left(\frac{\hat{w}}{t}\right)^2$$

$$+ \frac{(1+\nu)k_1 t}{8}\left(\frac{\bar{E}_s}{\bar{E}}\right)\left(\frac{\bar{E}}{\sigma_0}\right)^2\left(\frac{\hat{w}}{t}\right)^2. \tag{12}$$

With ν and $\bar{E}_s/\bar{E}$ specified and $\sigma_0/\bar{E}$ determined from (1), U/U_0 can be computed from (12) for any $k_1 t$ because $\sigma_0^E/\bar{E} = (k_1 t)^2/12 + (\bar{E}_s/\bar{E})/(2 k_1 t)$ and $\hat{w}/t$ is given by (9). For the critical mode with $k_1 t \equiv k^C t = (3\bar{E}_s/\bar{E})^{1/3}$ and $\sigma_0^E = \sigma_0^C$ given by (6), one finds $\hat{w}/t = \sqrt{\sigma_0/\sigma_0^C - 1}$ and

$$\frac{U}{U_0} = \frac{1+\nu}{2}\left[\left(\frac{\sigma_0^C}{\sigma_0}\right)^2 + \frac{(1-\nu)^2}{(1-\nu^2)}\right] + (1-\nu)\frac{\sigma_0^C}{\sigma_0}\left(1 - \frac{\sigma_0^C}{\sigma_0}\right). \tag{13}$$

Plots of U/U_0 as a function of σ_0/σ_0^C are given in Fig. 4 for $\nu = 1/3$, $\nu_s = 0.48$, and $\bar{E}_s/\bar{E} = 4100$, representative of a gold film on a PDMS substrate. Results for the normalized energy are presented for five values of the wavelength ratio, $L/L^C = k^C/k_1$, where $L = 2\pi/k_1$ is the wavelength and $L^C \equiv 2\pi/k^C$ is the wavelength of the critical mode. The wavelength predicted for the gold film/PDMS substrate system is 3 μm which is significantly below the observed wavelength of roughly 20 to 30 μm seen in Figs. 1 and 2. The discrepancy, discussed in [1,2], is believed to be due to a layer of PDMS just below the film whose Young's modulus is much higher than the bulk elastomer due the high film deposition temperature. In effect, it is argued that there is a two-layer film whose thickness is substantially greater than the gold film. Other possibilities for the wavelength discrepancy include the possibility that the modulus used for PDMS in the range of very small strains applicable to this problem may not be correct. The experimental agreement with the theoretical wavelength prediction is considerably better in [3].

The results of Fig. 4 for U/U_0 for the one-dimensional mode show that the lowest energy state is associated with the critical mode ($L/L^C = 1$) even at finite amplitude buckling deflections. The lowest energy state at values of σ_0/σ_0^C just above unity must be associated with the critical mode, but, in general, there is no a priori reason why lowest energy configuration should remain as-
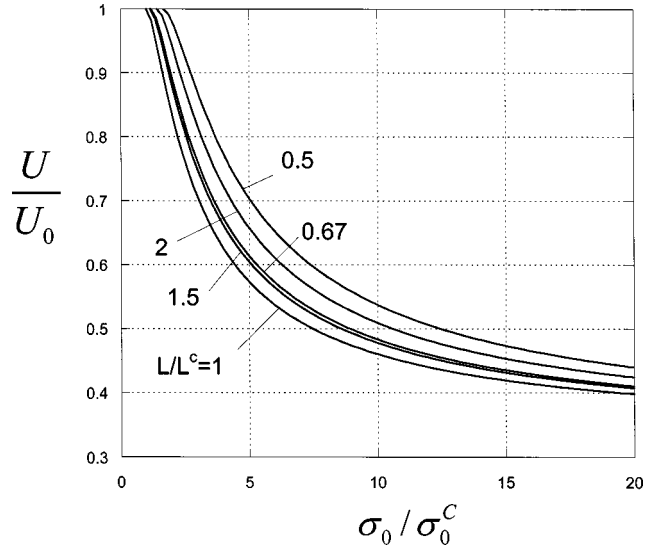

Fig. 4 Ratio of average elastic energy per unit area in the film/substrate system in the buckled state to that in the unbuckled state, U/U_0, as a function of σ_0/σ_0^C for the one-dimensional mode. Results are shown for several wavelengths. Note that the wavelength that is critical at the onset of buckling ($k_1 = k_1^C$) produces the minimum energy in the buckled state even when σ_0 is well above σ_0^C.

sociated with the critical mode. Thus, the results of Fig. 4 emphasize the strong preference for the wavelength associated with the critical wavelength $L^C \equiv 2\pi/k^C$ when the mode is one-dimensional. The limit of the energy ratio as σ_0/σ_0^C becomes large is $U/U_0 = (1-\nu)/2$. In this limit the in-plane compressive stress perpendicular to the buckles is completely relieved but the compressive stress parallel to the buckles is changed only by the Poisson effect.

4 Numerical Analysis of the Checkerboard and Herringbone Modes

An exact analytic solution such as that given for the one-dimensional mode cannot be obtained for either the checkerboard or the herringbone mode. The finite element code, ABAQUS, has been used to obtain a three-dimensional analysis of the periodic cell of these two modes. Within the cell, the plate is represented by 1000 three-dimensional eight-node, quadratic thin shell elements (with five degrees-of-freedom at each node and with reduced integration) that account for finite rotations of the middle surface. The stresses and strains within the plate are linearly related. The substrate is meshed with 20-node quadratic block elements with reduced integration. The constitutive relation of the substrate is also taken to be linear isotropic elasticity, but the geometry is updated. As mentioned earlier, nonlinear strain-displacement behavior of the substrate has essentially no influence on the results of interest. The substrate is taken to be very deep (depth d) compared to mode wavelength, and the boundary conditions along its bottom surface are zero normal displacement and zero tangential tractions. The film is assigned a temperature-independent thermal expansion mismatch, $\Delta\alpha$, and a temperature drop ΔT is imposed starting from the unstressed state. The biaxial compressive stress in the unbuckled film is therefore $\sigma_0 = E\Delta\alpha\Delta T/(1-\nu)$ if the substrate is infinitely deep. For each mode, a unit periodic cell is identified and meshed with periodicity conditions imposed on the edges of cell, both for the film and the underlying substrate.

4.1 The Square Checkerboard Mode. Consider a square checkerboard mode such that the wavelength L in the x_1 and
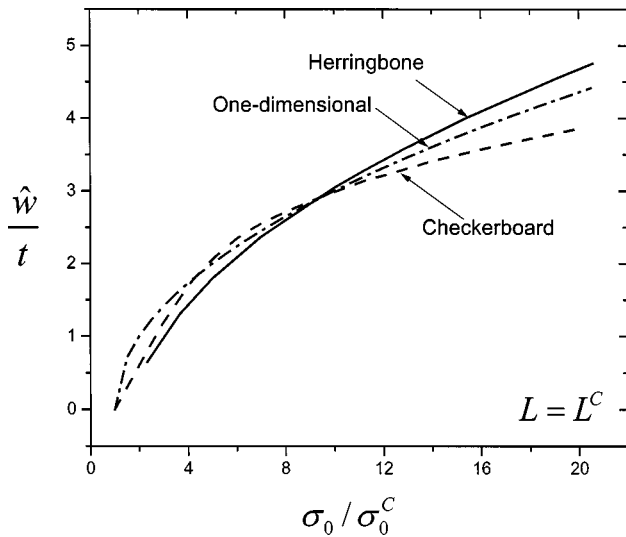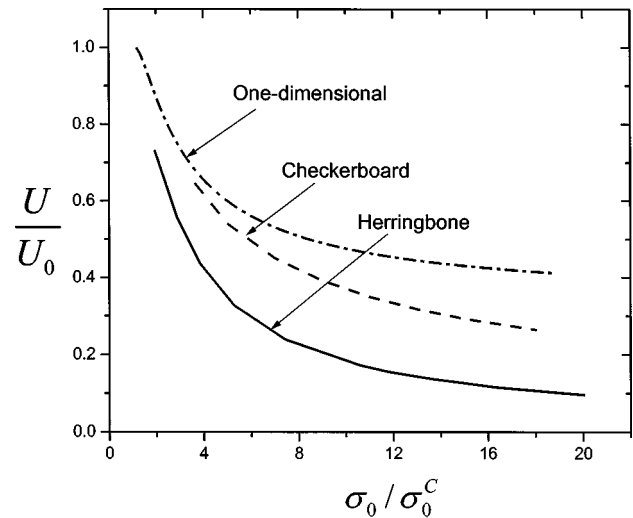
Fig. 5 Buckling amplitude of the film, $\hat{w}/t$, as a function of σ_0/σ_0^C for the three modes considered. The wavelengths (and inclination in the case of the herringbone mode) correspond to the critical at the onset of buckling.

Fig. 6 Ratio of average elastic energy per unit area in the film/substrate system in the buckled state to that in the unbuckled state, U/U_0, as a function of σ_0/σ_0^C for the three modes considered. The wavelengths (and inclination in the case of the herringbone mode) correspond to the critical at the onset of buckling. At σ_0/σ_0^C well above unity, the herringbone mode lowers the energy more than the other two modes.

x_2-directions is set by the critical condition in (7), i.e., $2\pi/k_1 = 2\pi/k_2 = L = \sqrt{2}L^C$ where as defined before $L^C \equiv 2\pi/k^C$. The unit cell in this case is a rectangular parallelepiped of dimension $L \times L \times d$. A very small initial imperfection is prescribed such that the plate in the unstressed system at $\Delta T = 0$ has a slight middle surface deflection, $w = \hat{w}_I \cos(k_1 x_1)\cos(k_2 x_2)$, where $\hat{w}_I/t = 0.02$. Periodicity conditions are applied to the cell by enforcing all five nodal degrees-of-freedom to be the same on the two edges of the cell parallel to the x_1-coordinate, and similarly for the x_2-axis. In addition, at one of the corners of the cell the conditions $\partial w/\partial x_1 = 0$ and $\partial w/\partial x_2 = 0$ are enforced such that the mode crests and valleys align with the cell sides.

A square checkerboard mode is indeed determined with normal deflection that is roughly of the form $w = \hat{w}\cos(k_1 x_1)\cos(k_2 x_2)$. The computed relation between the mode amplitude, $\hat{w}/t$, defined as one half the difference between the maximum and minimum deflections, and σ_0/σ_0^C is plotted in Fig. 5. Included in this figure are the corresponding results for the one-dimensional mode and the herringbone mode, which is obtained in the next subsection. The results for the computed average strain energy per area in the film/substrate system are presented in Fig. 6 in normalized form as U/U_0 versus σ_0/σ_0^C. The results for the one-dimensional mode with $k_1 = k^C$ ($k_2 = 0$) are also plotted, as is the corresponding result for the critical herringbone mode obtained next. The energy per area of the critical checkerboard mode lies between that for the one-dimensional mode and the herringbone mode.

4.2 The Herringbone Mode. The unit top surface of the periodic cell for the herringbone mode is shown in Fig. 7. The parallelepiped is characterized by its width, a, breadth, L, and inclination angle, α. Periodicity conditions are applied to the top and bottom edges of the cell, and symmetry is imposed on the left and right edges. A small initial deflection ($\hat{w}_I/t = 0.02$) satisfying these edge conditions is introduced to initiate the mode.
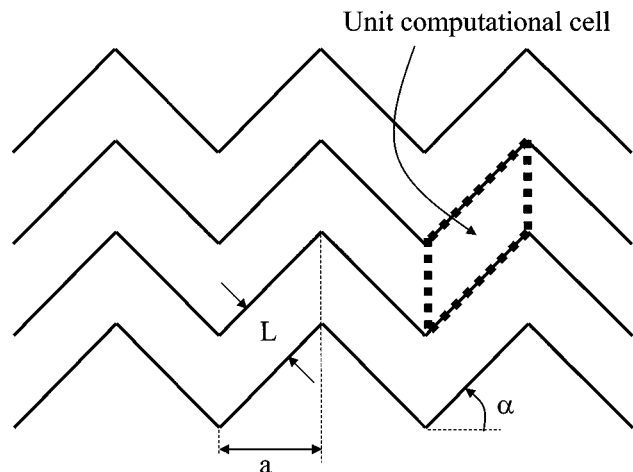
Contours of the normal deflection of the film w within the cell are displayed in Fig. 8 for three values of L/L^C, at $\sigma_0/\sigma_0^C = 26$ (Figs. 8(a), 8(b)) or $\sigma_0/\sigma_0^C = 4$ (Fig. 8(c)) with $a/L = 2$ and $\alpha = 45°$. It will be seen below that the minimum energy configuration has $L/L^C \cong 1$, and for this value it can be seen that the deflection shape displays the features of the herringbone mode seen in Figs. 1 and 2. The mode has a curving ridge running along the center of the cell that aligns itself to merge smoothly at the jog

with the ridge in the next cell. The excess breadth of the cell having $L/L^C = 2.4$ results in two ridges in the interior sector of the cell. The shape of the mode with narrow breadth, $L/L^C = 0.55$, is similar to that of the experimental herringbone pattern, but it will be seen that the energy for the narrow cell is well above that for $L/L^C = 1$.

The dependence of U/U_0 on the parameters of the cell geometry ($L/L^C, a/L, \alpha$) is presented in Fig. 9. Figure 9(a), displays the clear trend whereby minimum energy is associated with $L/L^C \cong 1$. The energy of modes with $L/L^C = 1.6$ and $L/L^C = 0.7$ is distinctly above the minimum. In Fig. 9(b) it is seen that the energy in the buckled state is surprisingly insensitive to the normalized length of the cell, a/L. Only for very short cells, $a/L = 0.5$, is the energy noticeably above the minimum. Evidence for this insensitivity is reflected in the experimental herringbone patterns in Figs. 1 and 2, where it can be seen that the distance between jogs varies by at least a factor of two from one section of the film to another. Similarly, there is not a very strong dependence of the energy of the buckled system on the inclination of the cell, α, although the
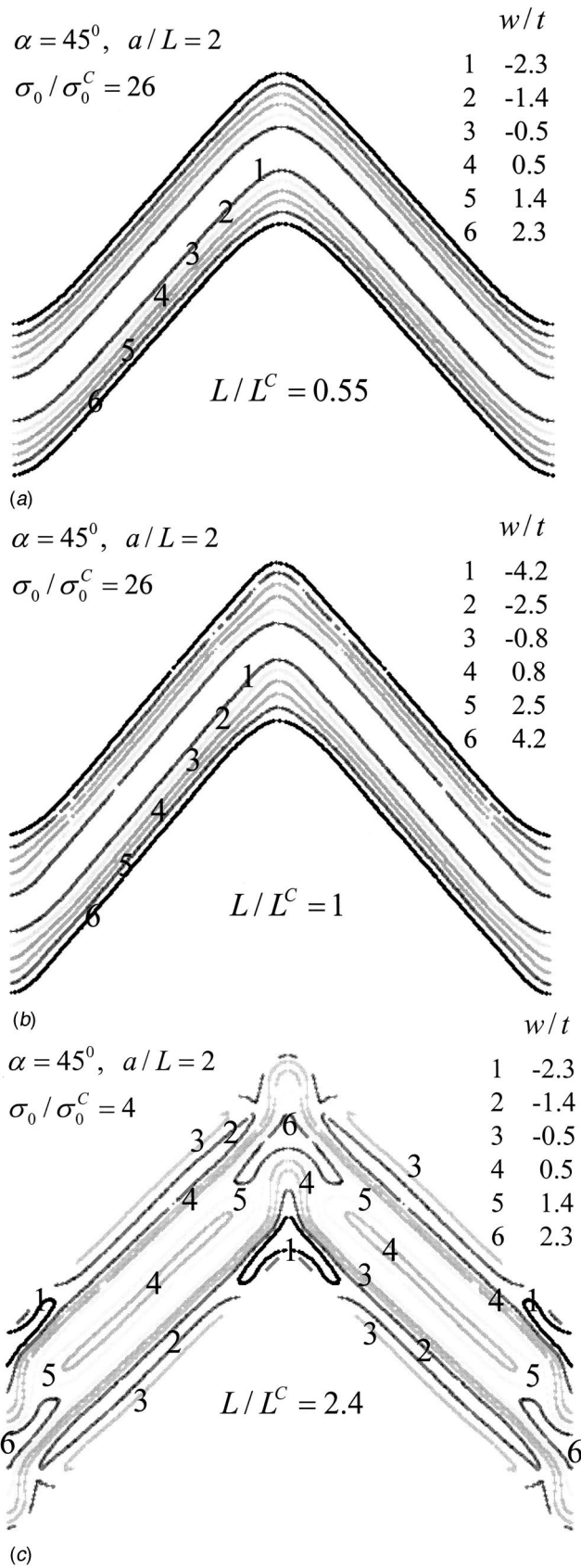

Fig. 7 Periodic cell of the herringbone mode

$\alpha = 45^0, \quad a/L = 2$

$\sigma_0/\sigma_0^C = 26$

	w/t
1	-2.3
2	-1.4
3	-0.5
4	0.5
5	1.4
6	2.3

$L/L^C = 0.55$

(a)

$\alpha = 45^0, \quad a/L = 2$

$\sigma_0/\sigma_0^C = 26$

	w/t
1	-4.2
2	-2.5
3	-0.8
4	0.8
5	2.5
6	4.2

$L/L^C = 1$

(b)

$\alpha = 45^0, \quad a/L = 2$

$\sigma_0/\sigma_0^C = 4$

	w/t
1	-2.3
2	-1.4
3	-0.5
4	0.5
5	1.4
6	2.3

$L/L^C = 2.4$

(c)

Fig. 8 Contour plots of the normal deflection of the film in the herringbone mode at $\sigma_0/\sigma_0^C=26$ (a,b) and $\sigma_0/\sigma_0^C=4$ (c) for several values of the breadth of the periodic cell, all with $a/L=2$ and $\alpha=45$ deg
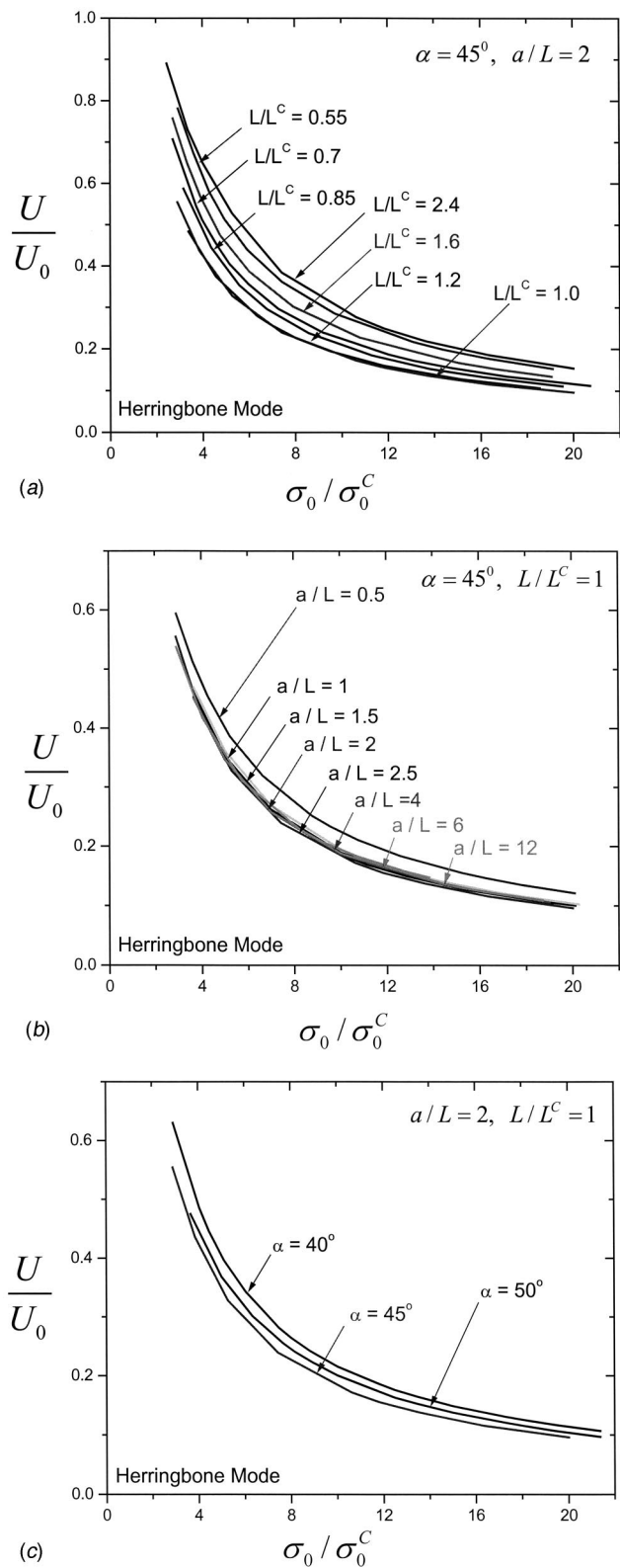

(a)

(b)

(c)

Fig. 9 Variation of U/U_0 as a function of σ_0/σ_0^C for the herringbone mode. (a) Dependence on L/L^C with $a/L=2$ and $\alpha=45$ deg. (b) Dependence on a/L with $L/L^C=1$ and $\alpha=45$ deg. (c) Dependence on α with $L/L^C=1$ and $a/L=2$.

minimum is attained for $\alpha \cong 45$ deg (Fig. 9(c)). A feature seen in each of the plots in Fig. 9, as well as for the one-dimensional mode in Fig. 4, is the invariance of the ordering of the relative energy trends with respect to changes in σ_0/σ_0^C. Put another way, the parameters governing the geometry of the minimum energy mode do not change in a significant way as σ_0/σ_0^C increases. In both Figs. 5 and 9 the results for the herringbone mode are only plotted for values of σ_0/σ_0^C sufficiently large compared to unity. The herringbone mode is not a bifurcation mode, and it only becomes a preferred mode in the sense of having minimum energy at σ_0/σ_0^C somewhat above unity. At $\sigma_0/\sigma_0^C \approx 1$, the amplitude and normalized energy of the herringbone mode is dominated by the initial imperfection.

5 Conclusions

Among the three buckling modes considered, the herringbone mode produces the lowest average elastic energy of the film/substrate system for films stressed well above critical, as seen in Fig. 6. The herringbone mode is able to relax the biaxial pre-stress stress, σ_0, in the film in all directions while inducing relatively little concurrent stretch energy. The stretch energy associated with buckling that does occur is localized in the jog regions. By contrast, the one-dimensional mode requires essentially no stretch energy (it continues to exhibit zero Gaussian curvature), but it relaxes the biaxial pre-stress only in one direction. The checkerboard mode relaxes the pre-stress in all directions, but it develops non-zero Gaussian curvature and induces much more concurrent stretch energy than the herringbone mode. The minimum energy state of the herringbone mode has undulation width, L, which is very close to that of the one-dimensional mode, $L^C = 2\pi t(\bar{E}/3\bar{E}_s)^{1/3}$, and jog angle $\alpha \cong 45$ deg. The minimum energy state is weakly dependent on the spacing between jogs, where stretch is localized. The experimental herringbone patterns in Figs. 1 and 2 show a spread in the jog spacing, and they also displays jog angles in reasonable agreement with the theoretical minimum energy state.

A question not addressed in this paper is how the herringbone mode emerges as σ_0 increases above critical. For a small range of σ_0 above critical, combinations of the classical modes of Section 2 necessarily have the lowest system energy; but as σ_0 increases, the herringbone mode emerges as the minimum energy mode. Does the herringbone mode spread across the film starting from some region of imperfection or from an edge? Or does it somehow emerge spontaneously over the entire film as a transition from a combination of classical modes? Bowden et al. [1,2] were not able to observe the evolution of the buckling patterns as their specimens were cooled from the film deposition temperature, and thus at this time it is not possible to give an experimental description of how the herringbone mode evolves.

A word of caution is in order about predicting mode patterns based on minimum energy states. The means by which deformations evolve to the minimum energy state is by no means obvious. Mechanics is replete with problems whose minimum energy states are not easily assessable. The pattern formed by forcing a film to buckle into a mold in Fig. 3 is just such an example. Once the finite amplitude mode has formed and the mold removed, it appears that the mode is locked in place and does not undergo changes towards a lower energy state unless further disturbed. To our knowledge, the nonlinear mechanics governing such behavior in buckled films has not been studied. In the case of the minimum energy herringbone mode, experimental observation confirms its existence, even though it has not been established how it evolves.

References

[1] Bowden, N., Brittain, S., Evans, A. G., Hutchinson, J. W., and Whitesides, G. M., 1998, "Spontaneous Formation of Ordered Structures in Thin Films of Metals Supported on an Elastomeric Polymer," Nature (London), **393**, pp. 146–149.

[2] Huck, W. T. S., Bowden, N., Onck, P., Pardoen, T., Hutchinson, J. W., and Whitesides, G. M., 2000, "Ordering of Spontaneously Formed Buckles on Planar Surfaces," Langmuir, **16**, pp. 3497–3501.

[3] Yoo, P. J., Suh, K. Y., Park, S. Y., and Lee, H. H., 2002, "Physical Self-Assembly of Microstructures by Anisotropic Buckling," Adv. Mater. (Weinheim, Ger.), **14**, pp. 1383–1387.

[4] Timoshenko, S. P., and Gere, J. M., 1961, *Theory of Elastic Stability*, McGraw-Hill, New York.

[5] Allen, H. G., *Analysis and Design of Structural Sandwich Panels*, Pergamon, New York.